UC Davis

UC Davis Previously Published Works

Title

Riparian Methylmercury Production Increases Riverine Mercury Flux and Food Web Concentrations.

Permalink

https://escholarship.org/uc/item/7h35d1vh

Journal

Environmental Science & Technology, 58(46)

Authors

Krause, Virginia

Baldwin, Austin

Peterson, Benjamin

et al.

Publication Date

2024-11-19

DOI

10.1021/acs.est.4c08585

Peer reviewed

eScholarship.org Powered by the California Digital Library
University of California

Environmental Science & Technology

pubs.acs.org/est

Open Access

This article is licensed under CC-BY-NC-ND 4.0

Article

Riparian Methylmercury Production Increases Riverine Mercury Flux and Food Web Concentrations

Virginia M. Krause, Austin K. Baldwin, Benjamin D. Peterson, David P. Krabbenhoft, Sarah E. Janssen, James J. Willacker, Collin A. Eagles-Smith, and Brett A. Poulin*

Cite This: *Environ. Sci. Technol.* 2024, 58, 20490−20501

Read Online

ACCESS | Metrics & More | Article Recommendations | Supporting Information

ABSTRACT: The production and uptake of toxic methylmercury (MeHg) impacts aquatic ecosystems globally. Rivers can be dynamic and difficult systems to study for MeHg production and bioaccumulation, hence identifying sources of MeHg to these systems is both challenging and important for resource management within rivers and main-stem reservoirs. Riparian zones, which are known biogeochemical hotspots for MeHg production, are understudied as potential sources of MeHg to rivers. Here, we present a comprehensive quantification of the hydrologic and biogeochemical processes governing MeHg concentrations, loads, and bioaccumulation at 16 locations along 164 km of the agriculturally intensive Snake River (Idaho, Oregon USA) during summer baseflow conditions, with emphasis on riparian production of MeHg. Approximately one-third of the MeHg load of the Snake River could not be attributed to inflowing waters (upgradient, tributaries, or irrigation drains). Across the study reach, increases in MeHg loads in surface waters were significantly correlated with MeHg concentrations in riparian porewaters, suggesting riparian zones were likely an important source of MeHg to the Snake River. Across all locations, MeHg concentrations in surface waters positively correlated with MeHg concentrations in benthic snails and clams, supporting that riparian produced MeHg was assimilated into local aquatic food webs. This study contributes new insights into riparian MeHg production within rivers which can inform mitigation efforts to reduce MeHg bioaccumulation in fish.

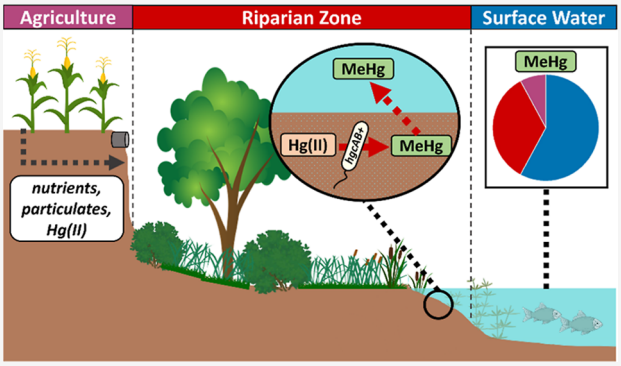

KEYWORDS: *methylation, load, agriculture, biogeochemical processes, Snake River*

1. INTRODUCTION

Mercury (Hg) is a pervasive global contaminant[1] with adverse effects on ecosystems and human health. Hg poses a significant global challenge due to its long atmospheric residence time that leads to global dispersion[2] and ability to undergo a key environmental transformation to form neurotoxic methylmercury (MeHg)[3] that can bioaccumulate and biomagnify to toxic levels in aquatic ecosystems.[4] The cycling of Hg initiates with the release of inorganic Hg (Hg(0), Hg(II)) into the environment, where anthropogenic activities (e.g., mining, fuel combustion) have resulted in a 7-fold increase in atmospheric concentrations relative to natural sources (e.g., volcanoes, rock weathering).[5,6] Atmospheric Hg is delivered through wet and dry deposition to terrestrial and aquatic environments,[5] where it can undergo methylation to MeHg by diverse microorganisms in aquatic systems under suboxic and hypoxic conditions (i.e., conditions where dissolved O_2 is below saturation or <0.5 mg/L, respectively).[7−9] Rivers are critical environments for transport[10−13] and uptake of MeHg in food webs,[14] with nearly 80% of all river fish consumption advisories involving mercury across the United States.[15] Agricultural practices, with associated water uses, storage, and nutrient and organic carbon loads from agricultural returns, are recognized to impact riverine biogeochemical processes globally[15,16] and may facilitate MeHg production and accumulation in these vulnerable watersheds.[17] Understanding the impact of management and anthropogenic alteration of riverine environments on Hg cycling and methylation (e.g., dam impoundments, agricultural withdrawals, nutrient inputs)[18] is vital to addressing issues of MeHg uptake in aquatic food webs.

Within riverine systems, riparian zones play a crucial role on hydrologic and biogeochemical processes, as they are highly efficient at capturing fine sediments and nutrients from agricultural runoff,[19−21] acting as natural buffers in highly irrigated landscapes.[22−24] The elevated nutrient capture and inundated riparian sediments tends to promote warmer water

Received: August 16, 2024
Revised: October 28, 2024
Accepted: October 29, 2024
Published: November 8, 2024

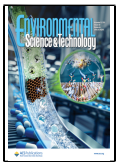

© 2024 The Authors. Published by American Chemical Society

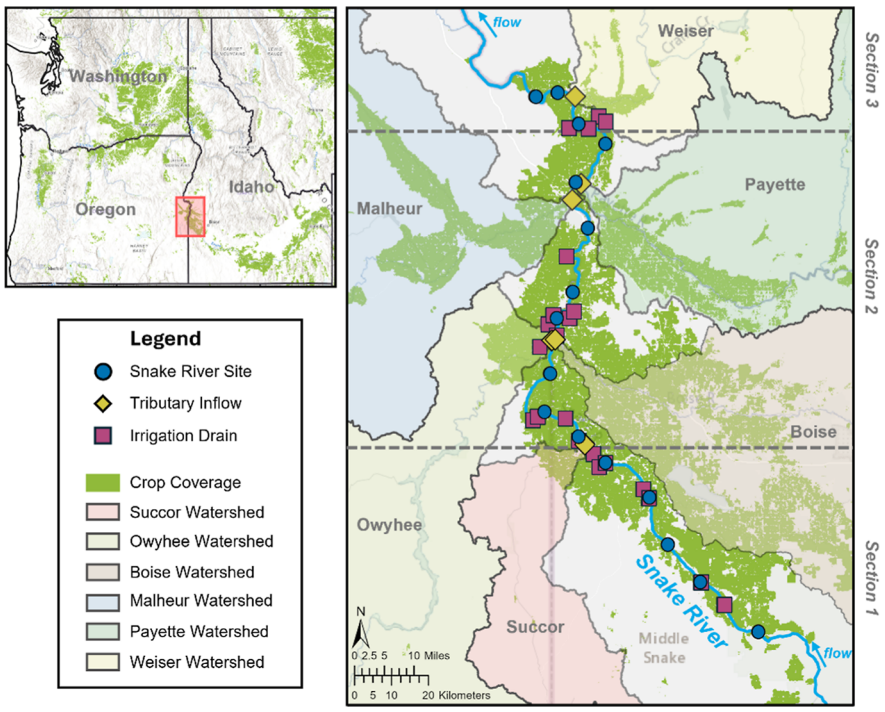

Figure 1. Map of Snake River synoptic survey conducted in July 2022; markers indicate locations of sample collection of main stem surface and pore waters (blue circles), tributary inputs (yellow diamonds), and irrigation drains (purple squares). Shaded regions represent major tributary watersheds and agricultural land coverage. Sections 1−3 are identified by the horizontal dashed lines.

temperatures and limited through-flow, which contribute to anoxic conditions and the prevalence of anaerobic processes.[22,25] These conditions establish riparian zones as dynamic biogeochemical hotspots at the interface of terrestrial and aquatic ecosystems.[22,25,26] These hotspots often include suboxic and anoxic conditions that facilitate microbial Hg(II) methylation, resulting in elevated MeHg production[27] and subsequent exchange or transport to neighboring surface waters.[11−13] In addition, these zones function as important sinks for terminal electron acceptors, such as sulfate (SO_4^{2-}),[28−31] which enhances microbial metabolism often linked to Hg(II) methylation.[7−9] In agricultural regions, microbial activity and variation in hydrologic inputs within riparian zones can also alter the concentration and composition of dissolved organic matter (DOM),[32,33] often characterized as the aromaticity using the specific ultraviolet absorbance at 254 nm ($SUVA_{254}$).[34] DOM plays a crucial role in riverine Hg transport and transformation.[35−37] Specifically, more aromatic DOM has been shown to transport more Hg per unit of DOC[38,39] and facilitate the formation of MeHg.[40,41] Thiol groups in DOM are strong Hg ligands[42−44] and impact the bioavailability of both Hg(II) for methylation,[40,45] and MeHg for biotic uptake to the food web.[46] In highly reducing conditions within the riparian soils and pore waters, formation of inorganic sulfide (S(-II)) from dissimilatory sulfate reduction[13,30,31] can outcompete Hg(II)-DOM binding, resulting in the formation of nanocolloidal metacinnabar (β-HgS).[27,47]

The complex relationships between redox gradients, microbial activity, and nutrient dynamics in riparian zones establishes them as likely hotspots for transformation, mobilization, and transport of Hg(II). However, the role of riparian zone processes in the formation of MeHg is understudied and poorly constrained. For example, an analysis of MeHg loads in the Snake River, a riverine system upgradient of a large reservoir complex, identified that 29−31% of the filter-passing MeHg (f.MeHg) and 38−40% of the particulate MeHg (p.MeHg) could not be accounted for by the main flows and inputs to the river, raising the possibility that riparian production is a major source of riverine MeHg loads.[48]

In this study, we quantified the sources and loads of MeHg along 164 km of the Snake River upgradient of a 3-reservoir hydroelectric complex, with an emphasis on riparian sources. Surface water flows and concentrations of constituents relevant to Hg cycling were measured at 16 sites along the Snake River and loads were quantified in surfaces water, tributaries, and irrigation drains. Further, a comprehensive assessment of riparian sediments and pore waters was carried out to test the hypothesis that riparian zones were a significant source of MeHg to the Snake River. Aquatic biota (i.e., clams, snails) were collected along the reach of the Snake River to assess if increases in stream MeHg concentrations corresponded with enhanced uptake of MeHg in the aquatic food web. The synoptic study, which evaluates a snapshot in time, highlights riparian zone contributions of MeHg to riverine surface waters and uptake in the aquatic food web, which can inform the implementation of land and water management actions to reduce MeHg uptake in fish, and thus potential MeHg exposure to consumers.

2. METHODS

2.1. Study Area. The Snake River, a major tributary of the Columbia River, runs through the southern regions of Idaho and eastern Oregon.[49,50] Land neighboring the study reach is heavily utilized for agriculture, with a high density of irrigation diversions and return drains scattered across the river basin.[48,50,51] Nearly 85% of the irrigated acreage in the entire State of Idaho is on the Snake River Plain.[51] The irrigation

https://doi.org/10.1021/acs.est.4c08585
Environ. Sci. Technol. 2024, 58, 20490−20501

infrastructure along the river basin contributes to excess nutrients and suspended solids.[48,50,51] The irrigated landscape and main stem of the Snake River are separated by narrow riparian zones that support a diverse range of vegetation.[52] Our investigation of the 164 km stretch of the Snake River provides a comprehensive understanding of the intricate dynamics within the region. All hydrologic inputs to the Snake River in the 164 km study area were divided into one of two categories: (i) major tributaries, which includes Succor Creek, Owyhee River, Boise River, Malheur River, Payette River, and Weiser River, or (ii) irrigation drains, which includes inputs that contain agricultural infrastructure (i.e., irrigation pump stations and return drains) (Figures 1 and S1) and minor tributaries and springs. Irrigation drains and minor tributaries were grouped together for analysis due to the interconnected nature of the diversions and return waters, making it difficult to identify their contributions separately, aligning with the classification established by Baldwin et al. (2024).[48]

2.2. Sample Collection & Processing. Complete details for sample collection and processing are provided in the Supporting Information (Supporting Information, Section S1.1). The synoptic survey was conducted July 11−14, 2022, when Hg(II) methylation is expected to be relatively high based on observed seasonal concentrations of both f.MeHg and p.MeHg in the mainstem 3-reservoir complex of the Snake River (Hells Canyon Complex), in which the first reservoir reflects similar riverine characteristics to that of the inflowing Snake River.[53] This seasonal increase of Hg(II) methylation in summer months has been observed in many other riverine systems.[54,55] The main stem of the Snake River was sampled at approximately 10 km intervals (Figure 1). At each of these 16 main stem sampling sites, surface water was collected from cross sections of the main stem Snake River using the U.S. Geological Survey (USGS) Equal Width Index method (n = 1−2 per site, n = 18 total).[56] River flow and velocity were measured along these cross sections using an Acoustic Doppler Current Profiler. Average discharge measurements at each location are presented with the associated uncertainties using Q-Rev software.[57] A multiparameter sonde (Aqua TROLL 600) measured surface water turbidity, specific conductance, pH, oxidation−reduction potential (ORP), dissolved oxygen (DO), and temperature concurrent with discrete sample collection. Surface water samples were also collected from the six major tributaries (n = 1−2 per tributary, n = 7 total) and 24 irrigation return drains (n = 1 per drain) that were actively discharging into the Snake River at the time of sample collection, using either the Equal Width Index or grab method at their confluence with the Snake River. All surface water samples were collected in 2 L polyethylene terephthalate glycol (PETG) bottles using ultraclean trace metal protocols. Sample collection methods for each site are defined in Poulin et al. (2023).[58] All surface water samples were stored on ice and filtered within 24 h of collection (quartz fiber filters (QFF), 0.7 μm pore size, precombusted at 550 °C, Whatman), into bottles for quantification of dissolved organic carbon (DOC) concentration and DOM optical characterization, inorganic anions (chloride (Cl^-), nitrate (NO_3^-), sulfate (SO_4^{2-})), filter-passing acidified metals (manganese (Mn), iron (Fe)), and filter-passing total Hg (f.THg) and MeHg (f.MeHg). Preservation and storage of these samples are defined in the Supporting Information (Supporting Information, Section S1.1). QFFs were frozen (−80 °C) for measurement of total suspended solids (TSS), particulate total Hg (p.THg), and particulate MeHg (p.MeHg) analyses. Unfiltered acidified metal samples were also collected. Particulate organic carbon (POC) and particulate nitrogen (PN) samples were filtered (0.3 μM glass fiber filters, Advantec, GF7513MM) and stored frozen (−20 °C) until analysis.

At each of the 16 main stem sites, pore water was collected using a custom Teflon sipper and peristaltic pump through acid-cleaned Teflon tubing (see Supporting Information, Section S1.1.3 for more details). The sipper was inserted 10 cm below the sediment−water interface in the shallow riparian areas along the river edge. A flow-through cell and multiparameter meters were used to measure pore water temperature, pH, DO, specific conductance, and ORP. Pore water was filtered in-line (QFF, 0.7 μm pore size, precombusted at 550 °C, Whatman) directly into bottles for measurement of inorganic sulfide (S(-II), preserved at 50% volume/volume with sulfide antioxidant buffer), DOC concentration and DOM composition, inorganic anions, f.THg, and f.MeHg. Sediment cores (6.25 cm diameter core barrel, 7−20 cm depth) were collected at each of the 16 main stem sampling locations, and 2−3 depths were selected based on sediment stratigraphy and measured for sediment total Hg, MeHg, and loss on ignition (a surrogate for organic matter content). Biota samples, collected with a benthic suction dredge near the riparian sampling areas, included submerged macrophytes, clams, and snails analyzed for total Hg and MeHg.

2.3. Sample Analyses. Complete details on sample analyses are provided in the Supporting Information (Supporting Information, Section S1.2). In brief, water samples were analyzed in the Poulin Lab at the University of California, Davis (Davis, CA) for concentrations of filter-passing and particulate metals (Fe, Mn), inorganic anions (Cl^-, NO_3^-, SO_4^{2-}), inorganic sulfide (S(-II)), DOC, and for DOM optical characterization ($SUVA_{254}$, spectral slope ratio (S_R)). The U.S. Geological Survey (USGS) Reston Stable Isotope Laboratory (Reston, VA) conducted POC and PN measurements on the collected glass fiber filters. The USGS Mercury Research Laboratory (Madison, WI) performed all mercury measurements (total Hg and MeHg) on the water samples (filter-passing and particulate), sediments, and macrophytes and loss on ignition on sediments, a proxy for total organic matter content. Inorganic divalent Hg (Hg(II)) concentrations, both filter-passing and particulate, were calculated by subtracting MeHg from total Hg concentrations (eq S1). Gravimetric Hg(II) and MeHg concentrations were calculated by dividing their volumetric counterpart concentrations by TSS. Biota mercury measurements (total Hg and MeHg) were performed at the USGS Contaminant Ecology Research Laboratory (Corvallis, OR). A comparison of field replicates is provided in the Supporting Information (Supporting Information, Section S1.3). All data are available online.[58]

2.4. Load Calculations. Complete details on load calculations are provided in the Supporting Information (Supporting Information, Section S1.4). Briefly, surface water loads were calculated along the entire study area using an established method for synoptic surveys,[59] which permits estimating inputs of constituents from surface water inflows (e.g., tributaries) and inputs without measurable surface flow (e.g., riparian contributions). First, instantaneous loads (i.e., "measured loads") were calculated by multiplying the concentration of a given constituent by the measured discharge at each site (eq S2). Second, the net change in load was determined between each of the discrete sampling locations

https://doi.org/10.1021/acs.est.4c08585
Environ. Sci. Technol. 2024, 58, 20490−20501

from upgradient to downgradient (eq S3); a positive value indicates a net gain in load between sites and a negative value indicates a net loss. Third, all net gains (excluding any loss terms) along the reach were added together to define a cumulative total for the synoptic, which is defined as the estimated "cumulative instream load" for the river (eq S4). This cumulative instream load provides a minimum estimate of the constituent load added to the system.[59] It omits net negative terms (i.e., loss terms) on the basis that load estimations can be influenced by attenuation (i.e., loss terms), which mask gaining contributions from inflows or internal production. Because sections of the river with net losses may still have contributions of loads that are masked by loss terms, the cumulative instream load estimates are a conservative estimate of constituent inputs and/or production.[59] The contributions from the tributaries were determined through calculation of the "cumulative inflow load" at each location (eq S5), by adding the instantaneous measured loads of each tributary to the Snake River starting load at the confluence. The cumulative inflow load provides an assessment of how much the inflowing tributaries account for the observed increases in the cumulative instream load.[59] Differences between the cumulative instream load, which represents the total surface water river load, and cumulative inflow load, which represents the tributary loads, denote an unaccounted (i.e., missing) load contribution not associated with the tributary inflows.[59]

2.5. Data Analysis. All data were analyzed and visualized using Microsoft Excel[60] and R statistical computing (2023.03.1-446) software.[61] Particulate metal concentrations (Fe, Mn) were calculated by subtracting the filter-passing concentrations from the unfiltered concentrations. Field replicates across the sample sites were averaged, and the mean value and associated minimum and maximum observed values for each replicate pair were used in data presentation. The error in measured instantaneous loads was estimated by error propagation using the error in discharge measurements. Concentrations reported below the detection limits (n = 1 for pore water SO_4^{2-}; n = 2 for pore water NO_3^-) were substituted at one-half the detection limit for data analyses and presentation. Comparisons of concentrations across sample types (e.g., surface waters vs pore waters) were performed using one-way analysis of variance testing (ANOVA or Kruskal–Wallis) and subsequent posthoc testing (Tukey–Kramer or Dunn's) depending on data distribution using the package *rstatix*.[62] Linear regression relationships were established using a linear model and evaluated for significance based on one-way analysis of variance testing (ANOVA) with the package *rstatix*.[62]

3. RESULTS & DISCUSSION

3.1. Hydrology. Surface water velocities were measured at all 16 main stem locations along the 164 km stretch. Velocity ranged from 0.27 to 0.72 m/s and displayed distinct hydrologic patterns in three sections: Section 1 (km 721.0–672.9) showed relatively consistent velocity, Section 2 (km 662.2–579.2) exhibited fluctuating velocity with a peak of 0.72 m/s, and Section 3 (km 571.7–556.5) showed a notable decrease in velocity associated with the transition from riverine to the more lacustrine environment above the first reservoir of the hydroelectric 3-reservoir complex (Hells Canyon Complex) (Figure S2A). Concurrently, discharge measurements revealed variations across designated sections: a decline in Section 1 attributed to irrigation withdrawals, a significant increase in Section 2 due to major tributary inflows, and relatively consistent flows in Section 3 (Figure 2A). Overall discharge at the downgradient end of the river reach was 229.4 m^3/s, with inflowing main stem and tributaries contributing 216.5 m^3/s, leaving a minor unaccounted portion of 5.6% in the hydrologic budget (Figure S2B). A more detailed assessment of the hydrology (Supporting Information, Section S3) estimated the contribution of irrigation drains, which further reduced this unaccounted portion and confirmed a near complete accounting (99.7–101%) of the hydrologic budget along the Snake River. This full accounting of the Snake River hydrologic budget enabled robust evaluation of sources and sinks of Hg and relevant biogeochemical constituents through the reach.

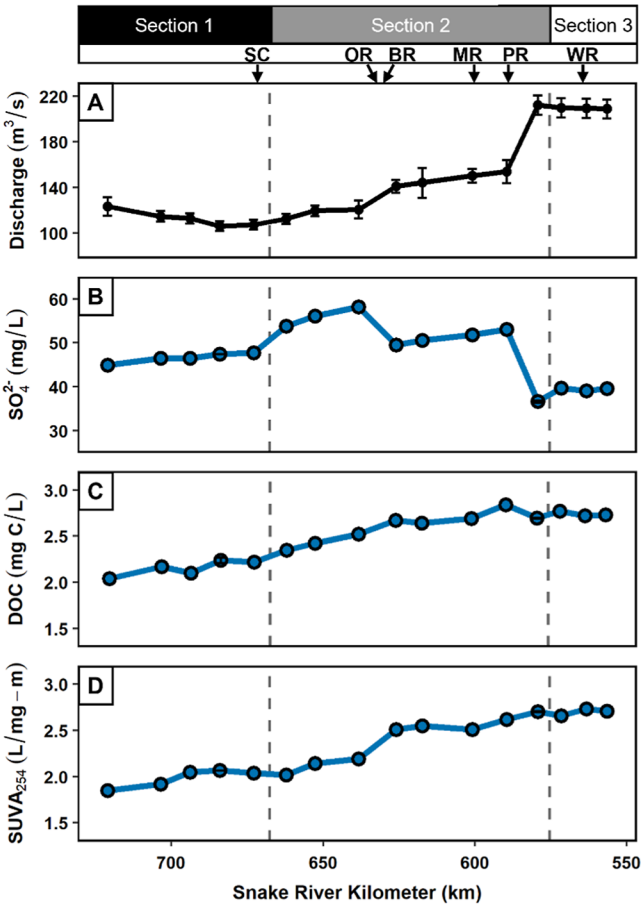

Figure 2. Hydrologic and biogeochemical trends through the study reach. Spatial trends across the main stem surface water for (A) discharge, (B) SO_4^{2-}, (C) DOC concentration, and (D) dissolved organic matter (DOM) specific ultraviolet absorbance at 254 nm ($SUVA_{254}$). Average concentrations are presented for field replicates with error bars presenting the minimum and maximum observed concentrations; some error bars are smaller than data symbols. Discharge (A) is presented with error bars that present the uncertainty of the measured discharge, determined by Q-Rev software.[57] Sections 1–3 are identified by the vertical dashed lines. Tributary confluence locations are presented as abbreviated names (SC = Succor Creek, OR = Owyhee River, BR = Boise River, MR = Malheur River, PR = Payette River, WR = Weiser River).

3.2. Surface Water Concentrations and Loads. *3.2.1. Pertinent Biogeochemical Constituents.* The surface waters of the Snake River exhibited strong spatial trends in the

https://doi.org/10.1021/acs.est.4c08585
Environ. Sci. Technol. 2024, 58, 20490–20501

distribution of biogeochemical constituents across the synoptic survey from up-to-down gradient, reflecting the upgradient Snake River with inflowing tributaries and irrigation drains. Concentrations of Cl^-, a conservative analyte, decreased stepwise along the river (Figure S3A) coincident with the confluences of the major tributaries in Section 2 of the transect. Although the median Cl^- concentrations in the main stem Snake River, tributaries, and irrigation drains (26.4, 17.9, 24.7 mg/L, respectively) were not statistically different (p-value > 0.05) (Figure S4A), the tributaries with high discharge were of lower Cl^- concentration thus diluting Cl^- in the main stem of the Snake River. In contrast, concentrations of NO_3^- and SO_4^{2-} were largely uniform in Section 1 and increased along the synoptic stretch in Section 2, likely due to agricultural influences from irrigation drains (Figures 1 and S1), with one major reduction in Section 3 due to dilution effects from the Malheur and Payette rivers (Figures S3C and 2B). Median concentrations of NO_3^- in the tributaries (0.83 mg NO_3^- (as N)/L) were marginally lower than the main stem Snake River (1.03 mg NO_3^- (as N)/L), and irrigation drains (2.86 mg NO_3^- (as N)/L) marginally higher, though not significant in either case (Figure S4B). Median concentrations of SO_4^{2-} in the tributaries and irrigation drains (59.1 and 70.4 mg/L, respectively) were marginally higher, though not significant, than the main stem Snake River (47.6 mg/L) (Figure S4C).

The measured loads of Cl^-, SO_4^{2-}, and NO_3^- decreased in Section 1 and increased in Sections 2 and 3 (Figure S5A−C). Similarly, the cumulative instream loads, which only account for positive load contributions between sites up-to-down gradient, were static in Section 1 and increased in Sections 2 and 3. Lastly, the cumulative inflow loads in the Snake River, which accounts for the tributary inputs, increased at locations downstream of the confluences of the six major tributaries. The cumulative instream loads of Cl^-, SO_4^{2-}, and NO_3^- all exceeded the cumulative inflow loads (Figure S5A−C), which indicates there are inputs of these constituents, primarily in Section 2 (between km 662.2−579.2), beyond the major tributaries. The cumulative inflow load could account for 86.7%, 73.4%, and 67.0% of the Cl^-, SO_4^{2-}, and NO_3^- across the reach of the synoptic survey, respectively. Contributions of inorganic anions from irrigation drains were assessed using an estimate of irrigation drain discharge along this stretch of the Snake River (13.7 ± 1.4 m^3/s)[48] and the average measured constituent concentrations of irrigation drains (n = 24). We estimate inputs from irrigation drains to account for 7.7% of the total Cl^- load, 15.2% of the total SO_4^{2-} load, and 20.5% of the total NO_3^- load. With the estimated inputs from agricultural drains, we can account for 94.3%, 88.6%, and 87.4% of the increases in loads of Cl^-, SO_4^{2-}, and NO_3^-, respectively, across the 164 km reach of the Snake River.

DOC exhibited a modest increase in concentration across the synoptic survey (from 2.04 to 2.73 mgC/L), showing no major influences from dilution effect from tributary inputs (Figure 2C). The DOM $SUVA_{254}$ followed the same trend, with an increase from 1.85 to 2.71 L/mgC m through the study reach (Figure 2D), and the spectral slope ratio (S_R)[63] decreased marginally (from 1.17 to 1.04) (Figure S6A). These trends indicate increases in DOC concentration and shifts in DOM composition to more aromatic from up-to-down gradient, which in-turn will influence the transport[11−13] and bioavailability of Hg(II)[40,45] and MeHg.[46] The measured load of DOC followed a similar trend to that of the anions, where the measured load decreased in Section 1, increased in Section 2, and plateaued in Section 3 (Figure S5D). The cumulative instream load of DOC remained constant through Sections 1 and 3, and only increased in Section 2. Cumulative inflow loads of DOC followed a similar pattern, but with minor increases in Section 3 (Figure S5D). The cumulative inflows account for 88.0% of the total DOC load through the reach of the synoptic survey, and irrigation drains were estimated to contribute 7.3% of the total load based on measured DOC (Figure S5D) and estimates of irrigation drain flow.[48] Only 4.7% of the DOC load was not attributed to the surface water inflows, tributaries, or irrigation drains.

The particulate concentrations and loads in the Snake River exhibited contrasting behavior to the above-mentioned trends in filter-passing constituents. Spatially, TSS concentrations increased 2.7-fold along the 164 km of the Snake River (Figure S7A) coinciding with observed increases in surface water velocity (Figure S8), which can resuspend sediments and other particles that contribute to elevated TSS. TSS concentrations were significantly higher in the irrigation drains relative to the main stem surface waters (109 vs 24.6 mg/L, respectively; p-value < 0.001; Figure S9A), which supports the hypothesis that irrigation drains contribute to the particulate concentrations and loads.[48] POC concentrations followed a similar increasing trend (2.1-fold increase) along the reach of the synoptic survey (Figure S7B). Concentrations of POC were higher in both the tributaries and irrigation drains (1.51 vs 1.95 mg/L, respectively; p-value < 0.05) relative to the main stem surface waters (0.80 mg/L; Figure S9B). Our load analysis of the particulate constituents (TSS, POC) showed the same spatial trends observed for filter-passing constituents, with static cumulative instream and inflow loads through Section 1 and increases of load in Sections 2 and 3 (Figure S10). The measured load, however, decreased in Section 3 for both TSS and POC, which we associate with particle settling as the river velocity declined near the inflow of the reservoir complex (Figures S2A and S8). Unlike the filter-passing constituents presented above, a much larger discrepancy was observed between the cumulative instream and inflow loads for the TSS and POC across the study reach. Only 67.3% of the estimated total TSS load could be accounted for by the inflowing waters (main stem Snake River and tributaries, 38.7%) and irrigation drains (28.6%), with 32.7% of the load unaccounted (Figure S10A). For POC, 64.7% could be accounted for (53.5% from inflows, 11.2% from irrigation drains), with 35.2% of the load unaccounted (Figure S10B). We posit that these deficiencies in particulate loads are strongly associated with the dynamics of particle settling and resuspension in the main stem of the Snake River, as fluctuations in measured loads coincided with changes in river velocity (Figures S2A and S10). In summary, irrigation drains are a primary source of particulates to the Snake River that undergo settling and resuspension in surface waters.

3.2.2. Hg(II) and MeHg. Inorganic divalent mercury (Hg(II)) concentrations increased from upstream to downstream in the main stem Snake River in both filter-passing (f.Hg(II); from 0.23−0.52 ng/L) and particulate fractions (p.Hg(II); from 0.16−0.57 ng/L) (Figure S11A,B). Gravimetric p.Hg(II) concentrations also increased overall along the study reach (grav. p.Hg(II); from 18.9−25.4 ng/g) (Figure S11D). Concentrations of f.Hg(II) were significantly higher (p-value < 0.05) in the tributaries (1.00 ± 0.41 ng/L; avg ± stdev) and irrigation drains (1.15 ± 0.64 ng/L) than in main

https://doi.org/10.1021/acs.est.4c08585
Environ. Sci. Technol. 2024, 58, 20490−20501

stem surface waters (Figure S12A). Concentrations of p.Hg(II) were notably higher in the irrigation drains (5.99 ± 7.43 ng/L) relative to the main stem surface waters (Figure S12B), and the particulate fraction of Hg(II) was linked to the POC load (Figure S13B). The concentrations of f.Hg(II) in the surface waters correlated linearly (p-value < 0.001) with DOC (Figure S13A), attributed to the strong affinity of Hg(II) for thiol groups in organic matter,[43] as has been noted in the Snake River[48,53] and other riverine environments.[38,64,65]

Methylmercury (MeHg) concentrations—both the filter-passing (f.MeHg) and particulate (p.MeHg) fractions—increased in the main stem surface waters from up-to-down gradient within the Snake River (Figure 3B). The concentration of f.MeHg showed negligible net change between the starting and ending sampling locations (0.061 ng/L at the initial sample point, 0.062 ng/L at the final sample point), but large fluctuations were observed throughout the middle of the stretch, with a maximum concentration of 0.094 ng/L (Figure 3B). Concentrations of p.MeHg increased dramatically from the initial upgradient to final downgradient sampling locations, with a total 2.4-fold increase along the synoptic stretch (Figure 3B). Concentrations of p.MeHg were significantly higher (p-value < 0.05) in the tributaries (0.162 ± 0.080 ng/L) and irrigation drains (0.195 ± 0.208 ng/L) relative to the main stem surface waters (0.050 ± 0.030 ng/L), driven by the particulate load (Figures S10 and S12C). Gravimetric p.MeHg exhibited highly variable fluctuations in concentration throughout the study reach, with a decrease in Section 1 (from 3.45 to 1.75 ng/g) followed by an increase in Section 2 (from 1.75 to 3.17 ng/g) and minor changes in Section 3 (from 2.49 to 3.11 ng/g) (Figure S11E). Due to the importance of partitioning between aqueous and particulate phases of Hg(II) and MeHg, and the complications of differentiating trends of partitioning relative to other gains and losses on MeHg dynamics,[66,67] we evaluated trends in total MeHg concentration (f.MeHg + p.MeHg) across the surface waters compared to riparian pore water and sediment (Figure 3B–D). Total MeHg concentration started at 0.090 ng/L, exhibited a modest decrease in Section 1, increased to a maximum in Section 2 (0.170 ng/L), and then decreased in Section 3. The decrease in total MeHg in Section 1 (from 0.090 to 0.060 ng/L) is potentially driven by biotic and abiotic demethylation processes,[68] as well as minor hydrologic influences of particle settling. Decreases in Section 3 (from 0.161 to 0.132 ng/L) are primarily attributed to particle settling processes, as corroborated by velocity and particulate data (TSS, p.MeHg) (Figures S2A,S7,S8 and 3B). Overall, this variability in MeHg concentrations highlights the complexity of the hydrologic and biogeochemical factors along the river.

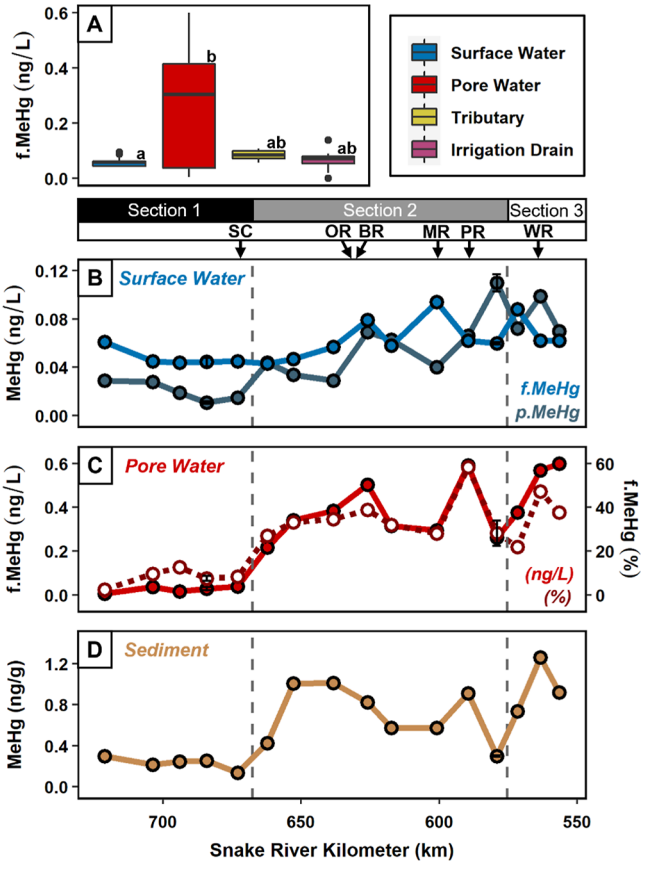

Figure 3. MeHg concentration (A) of all main stem surface waters, riparian pore waters, tributaries, and irrigation drains, and spatially in (B) main stem surface waters (blue), (C) riparian pore waters (solid red), and (D) riparian sediments (brown) over 164 km of the Snake River. In subplot C, the %MeHg is provided (dashed red). Average concentrations are presented for field replicates with error bars presenting the minimum and maximum observed concentrations; some error bars are smaller than data symbols. Sections 1–3 are identified by the vertical dashed lines. Tributary confluence locations are presented as abbreviated names (SC = Succor Creek, OR = Owyhee River, BR = Boise River, MR = Malheur River, PR = Payette River, WR = Weiser River).

Loads of filter-passing and particulate fractions of Hg(II) and MeHg exhibited similar trends across all Hg species (Figures 4 and S14). The measured loads of Hg(II) and MeHg (both filter-passing and particulate) decreased in Section 1, then increased in Section 2. In Section 3, the measured load of f.Hg(II) increased while all other measured loads of Hg fractions (p.Hg(II), f.MeHg, p.MeHg) decreased. The modest increase in f.Hg(II) load in Section 3 may be explained, in part, by oxidative MeHg demethylation in surface waters.[68] The cumulative instream load of each Hg species and fraction remained constant across Section 1 and increased in Section 2. Both the p.Hg(II) and f.MeHg cumulative instream loads were constant in Section 3, whereas f.Hg(II) and p.MeHg displayed minor increases. Cumulative inflow loads of Hg species and fractions followed a similar pattern to that of the instream loads, but at a lower magnitude.

We observed only 10.8% unaccounted load in the f.Hg(II), with 75.6% attributed to the upgradient Snake River and tributaries and 13.6% to the irrigation drains (Figure S14A). The unaccounted portion of f.Hg(II) (10.8%), though relatively minor, may be explained by uncertainty in our drain contributions based on estimations in flow for load analysis and/or associations to riparian production of DOC and processing of DOM.[33,35,36] Additional and unaccounted sources of f.Hg(II), such as groundwater seeps,[48] may also influence the load but were not accounted for here. Although loses of Hg(II) by photochemical reduction of Hg(II) to Hg(0) and subsequent volatilization were not measured,[69] it was considered of minor importance as the majority of f.Hg(II) load could be explained by hydrologic inputs (inflowing surface waters, tributaries, and irrigation drains) of the riverine system. Particulate Hg(II) exhibited a much larger unaccounted load at 28.5%, with 47.5% of the total load attributed to the upgradient Snake River and 28.9% attributed

https://doi.org/10.1021/acs.est.4c08585
Environ. Sci. Technol. 2024, 58, 20490−20501

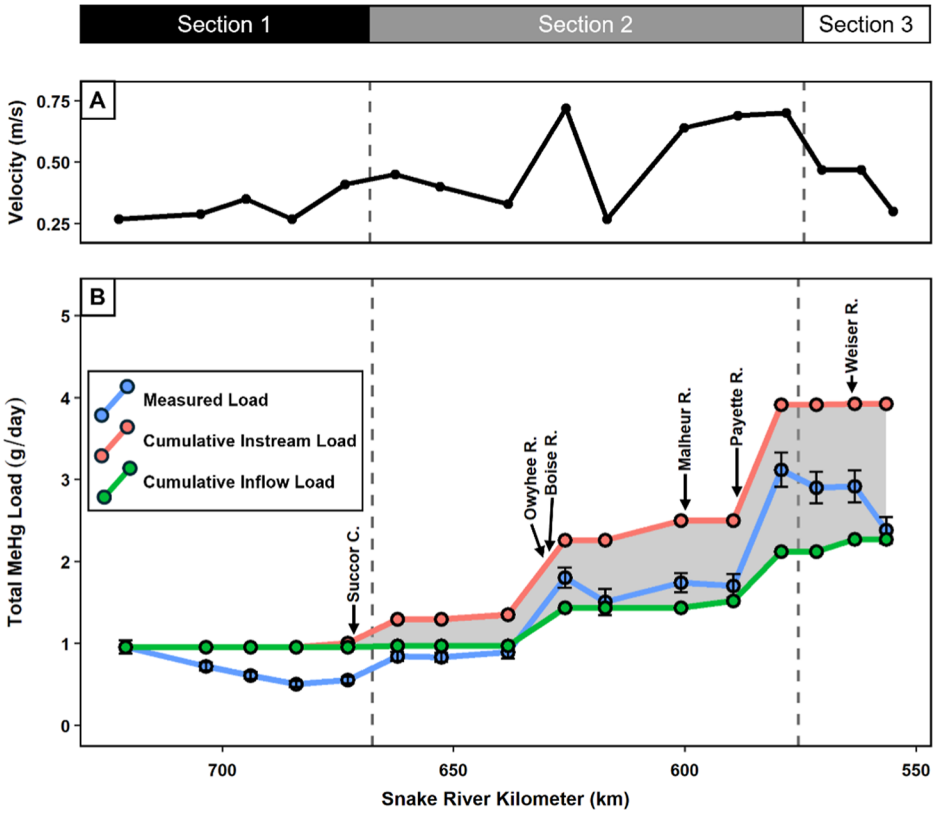

Figure 4. MeHg loadings along the study reach. (A) Velocities and (B) total MeHg loads of the Snake River including the cumulative instream (red), cumulative inflow (green), and measured instantaneous load (blue) over 164 km. In plot B, differences between cumulative instream and cumulative inflow represent the missing MeHg load, indicated by the shaded gray region. Sections 1−3 are identified by the vertical dashed lines. Propagated uncertainties associated with discharge measurements and replicate field measurements are shown with the measured load. Tributary names indicate their confluence point with the Snake River.

to the irrigation drains (Figure S14B). In summary, load comparisons confirm that hydrologic inputs and particle behavior govern filter-passing and particulate Hg(II) in the Snake River, with irrigation drains being a major source of p.Hg(II).

The unaccounted load for MeHg was much larger than that for Hg(II). When separated into filter-passing and particulate fractions, the analysis of f.MeHg identified 52.4% load contribution from the Snake River and major tributaries and only 3.1% contributions from the irrigation drains, leaving 44.5% missing source of f.MeHg (Figure S14C). In addition to the missing source of MeHg production, the river reach acted as an overall sink for f.MeHg, due to reasons detailed below. Particulate MeHg exhibited an even larger discrepancy, with only 30.9% load associated with the upgradient Snake River and tributaries and 7.3% with the irrigation drains, leaving 61.8% unaccounted (Figure S14D). Along the 164 km stretch of the Snake River, the total MeHg loads (Figure 4) displayed a decrease in Section 1, likely associated with water withdrawals for irrigation, notable increases in Section 2, and a modest decrease in Section 3. The decrease in the measured load of total MeHg in Section 3 aligns with marked decreases in velocity of the Snake River (Figure 4A) as it nears a downstream reservoir, resulting in particle settling. Both the cumulative instream and inflow loads of total MeHg in the surface waters present similar trends, with no change in load across Section 1, then increases in Section 2, then no change or minimal change in Section 3. A significant proportion of total MeHg could not be accounted for by hydrologic inputs in the surface waters. For the total MeHg load, 57.9% was from the upgradient Snake River and major tributaries and 7.9% was from the irrigation drains, with 34.2% unaccounted for (1.65 g/day) (Figure 4B). Overall, the unaccounted MeHg load is substantial and primarily attributed to gains in MeHg in Section 2 due to processes investigated below.

3.3. Riparian Pore Waters and Sediments as Location for MeHg Formation. The chemistry of the pore waters along the synoptic survey exhibited distinct zones characterized by a degree of suboxic conditions, sediment chemicals conditions, and microbial community composition, all of which played roles in shaping the biogeochemical environment. Riparian pore water NO_3^- concentrations were significantly lower ($0.03 \leq NO_3^- \leq 1.00$) ($p$-value < 0.05) than corresponding surface waters ($0.89 \leq NO_3^- \leq 1.30$; Figure S4B), with no spatial patterns along the stretch (Figure S3D). Spatially, pore water SO_4^{2-} showed high concentrations (>200 mg/L) at two locations in the upgradient sample sites, but concentrations at other locations were comparable to surface waters ($36.7 \leq SO_4^{2-} \leq 58.2$; Figures S15A and S4C). Sulfide (S(-II)) concentrations, attributed to dissimilatory SO_4^{2-} reduction in riparian sediments,[30] were highest in Section 1 ($0.42 \leq$ S(-II) ≤ 8.8 mg/L) and lower but above the detection limit (0.01 mg/L) in Section 2 and 3 ($0.11 \leq$ S(-II) ≤ 4.67 mg/L; Figure S15B). Further, pore water concentrations of filter-passing Fe and Mn (f.Fe, f.Mn) were significantly elevated compared to all the surface water samples (p-value < 0.05; Figure S16), interpreted to be the result of reductive dissolution of Fe(III) and Mn(IV/III) oxides.[70]

https://doi.org/10.1021/acs.est.4c08585
Environ. Sci. Technol. 2024, 58, 20490−20501

Collectively, these measurements reaffirm the existence of highly reduced riparian sediments throughout the 164 km reach of the Snake River. Riparian pore waters exhibited, in general, higher DOC concentrations (Figures S4D and S6C) and DOM of greater aromaticity (based on $SUVA_{254}$; Figure S6D)[34] and molecular weight (based on S_R; Figure S6B)[63] relative to surface waters. This may explain the observed monotonic increases in DOC concentration and DOM $SUVA_{254}$ in surface waters (Figure 2C,D) and increasing DOC loads (Figure S5D). These observations are consistent with previous studies on riparian DOM, which identify riparian zones as key areas for DOC export[32] and alteration of DOM composition.[33] Pore water f.Hg(II) concentrations increased steadily across the three sections of the Snake River, with a 5.2-fold increase across the synoptic survey (Figure S11C). Thus, riparian pore waters were reduced based on geochemical measurements and exhibited higher DOC concentration and greater DOM aromaticity, which leads to enhanced mobility (solubilization of particulate-bound Hg(II) to the aqueous state change) and bioavailability of Hg(II) for methylation by anaerobic microorganisms.[40,41,45]

Pore water concentrations of f.MeHg were significantly elevated compared to Snake River surface waters, irrigation drains, and tributaries (p-value < 0.05; Figure 3A) and increased systematically through the 164 km reach (Figure 3C) similarly to increases in surface water f.MeHg (Figure 3B). Pore water f.MeHg concentrations were low in Section 1 (f.MeHg ≤ 0.038 ng/L), showed a marked increase in Section 2 (0.22 ≤ f.MeHg ≤ 0.59 ng/L), and plateaued in Section 3 (0.38 ≤ f.MeHg ≤ 0.60; Figure 3C). The percentage of pore water total Hg as f.MeHg (%MeHg), a proxy for contemporary local MeHg production,[71−74] increased dramatically from 2.5% to 38% along the synoptic reach (Figure 3C). Spatial trends in sediment MeHg concentrations were similar to pore water f.MeHg trends, with low concentrations across Section 1, a 3.1-fold increase in Section 2, and relatively high but fluctuating levels in Section 3 (Figure 3D). The macrophytes collected within the riparian zones exhibited the same trend (Figure S17). Strong connectivity was observed across all riparian zones in MeHg concentrations (i.e., between pore waters, sediments, macrophyte) (Figure S18), and all reflect trends in net MeHg accumulation in the riparian zone along our study transect. While the contribution of MeHg from surface waters and associated macrophyte to pore water MeHg cannot be discounted, the sediment MeHg concentrations are most reflective of new MeHg production based on the high concentrations observed in the first 2 cm of the sediments (Figure S19) which maintained a high degree of connectivity to the pore waters. MeHg formation is likely facilitated by diverse microorganisms, as supported by the geochemical measurements of riparian pore waters (Figures S15 and S16) and environmental studies on the bacteria and archaea that possess the prerequisite *hgcAB* genes.[7−9] In summary, riparian pore waters and sediments in Section 2 exhibited elevated MeHg concentration (and % MeHg) that coincide with increases in surface water MeHg concentrations (Figure 3B) and the region of the river of increasing loads of MeHg not accounted for by tributary or agricultural drain inputs (Figure 4B).

The unaccounted load of MeHg at each of the 16 sites (Figure 4) correlated positively with the concentration of MeHg in the riparian pore waters (p-value = 0.0012; Figure 5A). In Section 1 of our synoptic stretch, concentrations and

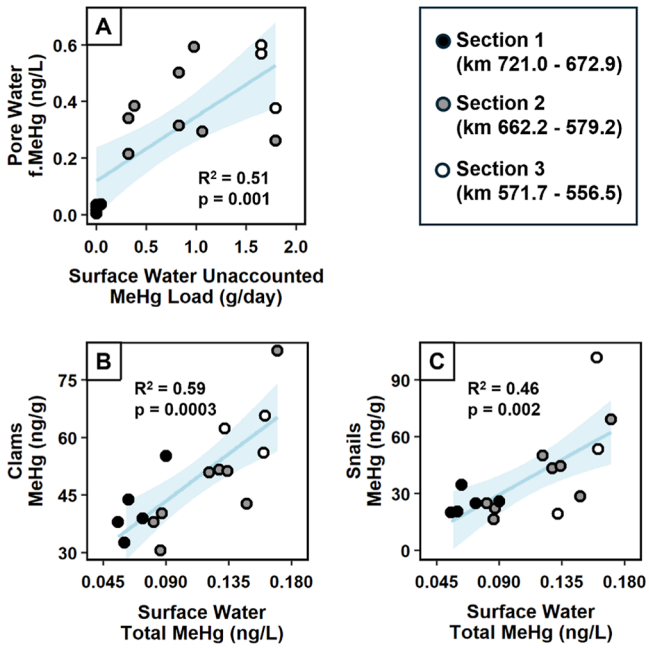

Figure 5. Linear correlations between MeHg sources in the study reach. Correlations between the (A) unaccounted load of MeHg in the main stem Snake River surface waters and the concentrations of MeHg in the riparian pore waters (p-value = 0.001), and the concentration of MeHg in the main stem surface waters to benthic (B) clams (p-value = 0.0003) and (C) snails (p-value = 0.002). The data point colors correspond to the sections of the Snake River in Figures 1−4: Section 1, Section 2, and Section 3. The blue line is the linear fit to observed data and shaded blue area correspond to the 95% confidence intervals of the fit.

loads of MeHg declined in surface waters attributed to sink processes (e.g., water withdrawals, particle settling), there was no unaccounted MeHg load, and riparian pore water were low in MeHg (black-filled symbols in Figure 5A). In Section 2, a strong positive correlation is observed between pore water f.MeHg concentration and the unaccounted surface water MeHg load (gray-filled symbols in Figure 5A). In Section 3, where pore water f.MeHg concentrations were relatively uniform, the data points closely reflected the overall regression trend (white-filled symbols in Figure 5A). Riparian sediment and macrophyte MeHg concentrations also correlated positively (p-value ≤ 0.038) with the unaccounted MeHg load in the main stem surface waters (Figure S20), although the coefficients of determination (R^2 values) were lower. Therefore, we attributed the missing cumulative 1.65 g MeHg/day in the Snake River to internal production within the riverine riparian zone (Figures 4 and 5A), which is a conservative estimate given that biotic and abiotic MeHg loss terms (e.g., photodemethylation) could not be accounted for and offset internal production. We cannot discount the possibility that the increase in MeHg load was influenced by MeHg formation in the hyporheic zone,[11−13] but this study did not measure hyporheic pore water. The findings reinforce the significance of riparian areas in MeHg production and transport.[75] We assert that MeHg formed in riparian pore waters is exchanged with surface waters through hydrologic forcing and molecular diffusion, which occurs at a slower rate than advective flow. This formation and exchange of MeHg is likely facilitated by Hg speciation, microbial activity, sediment composition, and partitioning behaviors of THg and MeHg

https://doi.org/10.1021/acs.est.4c08585
Environ. Sci. Technol. 2024, 58, 20490−20501

influenced by pore water DOC and S(-II).[66] The conclusions drawn here identify riparian zone production as the missing sources of MeHg identified in a previous investigation of the same section of the Snake River.[48]

It is unclear why MeHg concentrations in riparian pore waters and sediments exhibited clear zonation interpreted to reflect low (Section 1) and high Hg(II) methylation (Section 2) (Figure 3), as the riparian redox state, concentrations of terminal electron acceptors (NO_3^- and SO_4^{2-}), and by-products of heterotrophic microbial activity (f.Fe, f.Mn) were not drastically different in pore waters across the three sections of the river (Figures S3D,S15A and S16). Higher concentrations of f.Hg(II) in surface and pore waters in Section 2−3 (Figure S11B,C), driven by progressive increases in DOC concentration and DOM $SUVA_{254}$ (Figure 2C,D), may in part contribute to greater MeHg formation along this section of river. Further, the low MeHg levels in Section 1 may be explained by elevated S(-II) concentrations (Figure S15B), which could have been sufficiently high to inhibit Hg(II) methylation by promoting the formation of crystalline nanocolloidal β-HgS[47,76] of lower potential for methylation.[45] Although geochemical modeling was not performed here, the S(-II) and DOC concentrations of pore waters are within the range of conditions for which nanocolloidal β-HgS formation has been documented by X-ray absorption spectroscopy.[47,76] It is also possible that the microbial potential for methylation (i.e., *hgcAB* gene expression) was lower in Section 1 than Section 2, as has been shown to influence MeHg production in some natural and engineered wetlands.[41,77] Lastly, differences in hydrologic gradients (e.g., gaining vs losing reaches of the river) can be spatially variable depending on topography, connections to both local and regional groundwater systems, and proximity to locations of agricultural water withdrawal and application, all of which can impact the transport of Hg and MeHg into and out of the system.

3.4. MeHg Uptake in the Aquatic Food Web.

Concentrations of MeHg in filter-feeding and grazing benthic invertebrates (clams and snails, respectively) collected within riparian areas along the synoptic reach of the Snake River were significantly correlated (p-value < 0.05) to cocollected surface water MeHg concentrations (Figure 5B,C). The spatial trends in these biota thus followed similar trends as MeHg in surface water, riparian pore water, and sediment (Figures 3 and S21), with decreasing MeHg concentrations along Section 1 (clams: Figure S21A; snails: Figure S21B), increasing concentrations in Section 2, and a decline in Section 3. Bivalves are known to respond rather quickly to changes in MeHg availability[78,79] and assimilate aqueous MeHg as opposed to legacy sediment MeHg.[80] These correlations provide strong support of the assimilation of riparian-produced MeHg into Snake River aquatic food webs. Notably, correlations in both clams and snails support the incorporation of riparian derived MeHg into both particulate-based and periphyton-based portions of the food web, which together underpin most production in riverine systems, highlighting the importance of riparian MeHg production to subsequent exposure in higher trophic levels such as subsistence and recreationally harvested fish.[18]

4. IMPLICATIONS FOR RIVERINE SYSTEMS

This study presents a comprehensive assessment of the hydrologic and biogeochemical processes governing MeHg sources within a dynamic riverine system and identifies internal production of MeHg in riparian zones as a significant source of MeHg (34.2%) to the Snake River (Figure 4). Significant correlations were observed between the missing load and the concentrations of f.MeHg in the riparian pore waters (Figure 5A), and between concentrations of surface water MeHg and benthic organism MeHg (Figure 5B,C), confirming riparian zones are an important location for MeHg production and contributing source of MeHg to both the surface waters and local aquatic food webs. Inputs of POC, NO_3^- and SO_4^{2-} support highly reduced conditions in riparian areas along the Snake River and subsequent redox transformations and DOC production create methylation hotspots within the riparian zones, leading to enhanced production of MeHg that is exchanged with neighboring surface waters. Riparian zone production of MeHg contributed a minimum of 1.65 g MeHg/day to surface waters of the Snake River in summer, baseflow conditions, which equates to approximately 38% of the mean daily load of MeHg entering the downstream Brownlee Reservoir of the Hells Canyon Complex (~4.4 g/day),[49,53,81] Over the section of the Snake River with the greatest increase in MeHg load (Section 2), we estimate that 0.010 g MeHg·km^{-1}·day^{-1} of MeHg was produced under the observed flow conditions. The hydrologic inputs of inflowing surface waters (main stem surface waters and tributaries), and, to a lesser extent, irrigation drains to the Snake River were also contributing sources to MeHg loads (57.9 and 7.9% respectively). Irrigation drains were important sources of nutrients, DOC, and Hg(II) that could further promote microbial methylation within the anaerobic riparian zones of the river. The riparian production of MeHg can be an important source to riverine systems and may be a critical consideration in the development of management and mitigation efforts, such as nutrient reductions to limit the onset of anoxia or watershed stewardship programs, aimed at reducing MeHg in aquatic food webs, especially in regions with intensive agricultural activities influencing riparian zones.

■ ASSOCIATED CONTENT

Supporting Information

The Supporting Information is available free of charge at https://pubs.acs.org/doi/10.1021/acs.est.4c08585.

Sample collection, analyses, load calculations, irrigation withdrawal estimates, hydrologic budget, and figures (PDF)

■ AUTHOR INFORMATION

Corresponding Author

Brett A. Poulin − *Department of Environmental Toxicology, University of California—Davis, Davis, California 95616, United States;* orcid.org/0000-0002-5555-7733; Phone: +1 530 754 2454; Email: bapoulin@ucdavis.edu

Authors

Virginia M. Krause − *Department of Environmental Toxicology, University of California—Davis, Davis, California 95616, United States*

Austin K. Baldwin − *Idaho Water Science Center, U.S. Geological Survey, Boise, Idaho 83702, United States;* orcid.org/0000-0002-6027-3823

Benjamin D. Peterson − *Department of Environmental Toxicology, University of California—Davis, Davis, California 95616, United States;* orcid.org/0000-0001-5290-9142

David P. Krabbenhoft − *Upper Midwest Science Center, Mercury Research Laboratory, U.S. Geological Survey, Madison, Wisconsin 53726, United States;* orcid.org/0000-0003-1964-5020

Sarah E. Janssen − *Upper Midwest Science Center, Mercury Research Laboratory, U.S. Geological Survey, Madison, Wisconsin 53726, United States;* orcid.org/0000-0003-4432-3154

James J. Willacker − *Forest and Rangeland Ecosystem Science Center, U.S. Geological Survey, Corvallis, Oregon 97330, United States;* orcid.org/0000-0002-6286-5224

Collin A. Eagles-Smith − *Forest and Rangeland Ecosystem Science Center, U.S. Geological Survey, Corvallis, Oregon 97330, United States;* orcid.org/0000-0003-1329-5285

Complete contact information is available at: https://pubs.acs.org/10.1021/acs.est.4c08585

Notes

The authors declare no competing financial interest.

■ ACKNOWLEDGMENTS

The authors graciously acknowledge J. Pierce, B. Eachus, C. Rumrill, T. Glidden, B. Johnson, and the U.S. Geological Survey (USGS) Mercury Research Laboratory staff for assistance in aspects of sample collection, processing, and analysis. We thank D. George, E. Smith, R. Florence, and J. Carricaburu for collection of streamflow measurements. We thank B. Cook for assistance in data handling. Contributions to study planning and project discussions were made by N, Gastelecutto, B. Bean, R. Myers, J. Chandler, and J. Naymik. Funding and support were provided by Idaho Power Company, the Idaho Department of Environmental Quality, the University of California Agricultural Experimental Station (AES) Hatch project, Jastro & Shields Graduate Award, and the USGS Cooperative Funding, Toxic Substances Hydrology, and Contaminant Biology programs (Ecosystems Mission Area). Any use of trade, form, or product names is for descriptive purposes only and does not imply endorsement by the U.S. Government.

■ REFERENCES

(1) Driscoll, C. T.; Mason, R. P.; Chan, H. M.; Jacob, D. J.; Pirrone, N. Mercury as a global pollutant: sources, pathways, and effects. *Environ. Sci. Technol.* **2013**, *47* (10), 4967−4983.

(2) Sigler, J. M.; Lee, X.; Munger, W. Emission and long-range transport of gaseous mercury from a large-scale Canadian boreal forest fire. *Environ. Sci. Technol.* **2003**, *37* (19), 4343−4347.

(3) Hsu-Kim, H.; Kucharzyk, K. H.; Zhang, T.; Deshusses, M. A. Mechanisms regulating mercury bioavailability for methylating microorganisms in the aquatic environment: a critical review. *Environ. Sci. Technol.* **2013**, *47* (6), 2441−2456.

(4) *Handbook of Ecotoxicology*; Hoffman, D. J., Rattner, B. A., Burton, G. A., Cairns, J., Eds.; CRC Press, 2002.

(5) Selin, N. E. Global biogeochemical cycling of mercury: a review. *Annu. Rev. Environ. Resour.* **2009**, *34* (1), 43−63.

(6) Geyman, B. M.; Thackray, C. P.; Jacob, D. J.; Sunderland, E. M. Impacts of volcanic emissions on the global biogeochemical mercury cycle: insights from satellite observations and chemical transport modeling. *Geophys. Res. Lett.* **2023**, *50* (21), No. e2023GL104667.

(7) Gilmour, C. C.; Podar, M.; Bullock, A. L.; Graham, A. M.; Brown, S. D.; Somenahally, A. C.; Johs, A.; Hurt, R. A.; Bailey, K. L.; Elias, D. A. Mercury methylation by novel microorganisms from new environments. *Environ. Sci. Technol.* **2013**, *47* (20), 11810−11820.

(8) Peterson, B. D.; McDaniel, E. A.; Schmidt, A. G.; Lepak, R. F.; Janssen, S. E.; Tran, P. Q.; Marick, R. A.; Ogorek, J. M.; DeWild, J. F.; Krabbenhoft, D. P.; McMahon, K. D. Mercury methylation genes identified across diverse anaerobic microbial guilds in a eutrophic sulfate-enriched lake. *Environ. Sci. Technol.* **2020**, *54* (24), 15840−15851.

(9) Peterson, B. D.; Poulin, B. A.; Krabbenhoft, D. P.; Tate, M. T.; Baldwin, A. K.; Naymik, J.; Gastelecutto, N.; McMahon, K. D. Metabolically diverse microorganisms mediate methylmercury formation under nitrate-reducing conditions in a dynamic hydroelectric reservoir. *ISME J.* **2023**, *17* (10), 1705−1718.

(10) Brigham, M. E.; Wentz, D. A.; Aiken, G. R.; Krabbenhoft, D. P. Mercury cycling in stream ecosystems. 1. water column chemistry and transport. *Environ. Sci. Technol.* **2009**, *43* (8), 2720−2725.

(11) Bradley, P. M.; Journey, C. A.; Chapelle, F. H.; Lowery, M. A.; Conrads, P. A. Flood hydrology and methylmercury availability in coastal plain rivers. *Environ. Sci. Technol.* **2010**, *44* (24), 9285−9290.

(12) Bradley, P. M.; Journey, C. A.; Lowery, M. A.; Brigham, M. E.; Burns, D. A.; Button, D. T.; Chapelle, F. H.; Lutz, M. A.; Marvin-DiPasquale, M. C.; Riva-Murray, K. Shallow groundwater mercury supply in a coastal plain stream. *Environ. Sci. Technol.* **2012**, *46* (14), 7503−7511.

(13) Creswell, J. E.; Kerr, S. C.; Meyer, M. H.; Babiarz, C. L.; Shafer, M. M.; Armstrong, D. E.; Roden, E. E. Factors controlling temporal and spatial distribution of total mercury and methylmercury in hyporheic sediments of the Allequash Creek Wetland, Northern Wisconsin. *J. Geophys. Res. B* **2008**, *113* (G2), G00C02.

(14) Eagles-Smith, C. A.; Ackerman, J. T.; Willacker, J. J.; Tate, M. T.; Lutz, M. A.; Fleck, J. A.; Stewart, A. R.; Wiener, J. G.; Evers, D. C.; Lepak, J. M.; Davis, J. A.; Pritz, C. F. Spatial and temporal patterns of mercury concentrations in freshwater fish across the Western United States and Canada. *Sci. Total Environ.* **2016**, *568*, 1171−1184.

(15) U.S. Environmental Protection Agency. *National Rivers and Streams Assessment: The Third Collaborative Survey, EPA 841-R-22-004*; U.S. Environmental Protection Agency, Office of Water and Office of Research and Development, 2023. https://riverstreamassessment.epa.gov/webreport.

(16) Schürings, C.; Globevnik, L.; Lemm, J. U.; Psomas, A.; Snoj, L.; Hering, D.; Birk, S. River ecological status is shaped by agricultural land use intensity across Europe. *Water Res.* **2024**, *251*, 121136.

(17) Willacker, J. J.; Eagles-Smith, C. A.; Lutz, M. A.; Tate, M. T.; Lepak, J. M.; Ackerman, J. T. Reservoirs and water management influence fish mercury concentrations in the Western United States and Canada. *Sci. Total Environ.* **2016**, *568*, 739−748.

(18) Willacker, J. J.; Eagles-Smith, C. A.; Chandler, J. A.; Naymik, J.; Myers, R.; Krabbenhoft, D. P. Reservoir stratification modulates the influence of impoundments on fish mercury concentrations along an arid land river system. *Environ. Sci. Technol.* **2023**, *57* (50), 21313−21326.

(19) Aguiar, T. R., Jr.; Rasera, K.; Parron, L. M.; Brito, A. G.; Ferreira, M. T. Nutrient removal effectiveness by riparian buffer zones in rural temperate watersheds: the impact of no-till crops practices. *Agric. Water Manage.* **2015**, *149*, 74−80.

(20) Burns, D. A. Retention of NO_3^- in an upland stream environment: a mass balance approach. *Biogeochemistry* **1998**, *40* (1), 73−96.

(21) Lowrance, R.; Todd, R.; Fail, J., Jr.; Hendrickson, O., Jr.; Leonard, R.; Asmussen, L. Riparian forests as nutrient filters in agricultural watersheds. *BioScience* **1984**, *34* (6), 374−377.

(22) Vidon, P.; Allan, C.; Burns, D.; Duval, T. P.; Gurwick, N.; Inamdar, S.; Lowrance, R.; Okay, J.; Scott, D.; Sebestyen, S. Hot spots and hot moments in riparian zones: potential for improved water quality management. *J. Am. Water Resour. Assoc.* **2010**, *46* (2), 278−298.

(23) Lowrance, R. Effects of Buffer System on the Movement of N and P from Agriculture to Streams. *International Conference on N, P, and Organic Matter*, 1991. www2.mst.dk/Udgiv/publications/1991/87-503-9331-6/pdf/87-503-9331-6.pdf.

(24) Mander, Ü.; Kuusemets, V.; Lõhmus, K.; Mauring, T. Efficiency and dimensioning of riparian buffer zones in agricultural catchments. *Ecol. Eng.* **1997**, *8* (4), 299−324.
(25) McClain, M. E.; Boyer, E. W.; Dent, C. L.; Gergel, S. E.; Grimm, N. B.; Groffman, P. M.; Hart, S. C.; Harvey, J. W.; Johnston, C. A.; Mayorga, E.; McDowell, W. H.; Pinay, G. Biogeochemical hot spots and hot moments at the interface of terrestrial and aquatic ecosystems. *Ecosystems* **2003**, *6* (4), 301−312.
(26) Vidon, P. G.; Mitchell, C. P. J.; Jacinthe, P.-A.; Baker, M. E.; Liu, X.; Fisher, K. R. Mercury dynamics in groundwater across three distinct riparian zone types of the US Midwest. *Environ. Sci.: Processes & Impacts* **2013**, *15* (11), 2131−2141.
(27) Poulin, B. A.; Aiken, G. R.; Nagy, K. L.; Manceau, A.; Krabbenhoft, D. P.; Ryan, J. N. Mercury transformation and release differs with depth and time in a contaminated riparian soil during simulated flooding. *Geochim. Cosmochim. Acta* **2016**, *176*, 118−138.
(28) Compeau, G. C.; Bartha, R. Sulfate-reducing bacteria: principal methylators of mercury in anoxic estuarine sediment. *Appl. Environ. Microbiol.* **1985**, *50* (2), 498−502.
(29) Gilmour, C. C.; Henry, E. A.; Mitchell, R. Sulfate stimulation of mercury methylation in freshwater sediments. *Environ. Sci. Technol.* **1992**, *26* (11), 2281−2287.
(30) Küsel, K.; Alewell, C. Riparian zones in a forested catchment: hot spots for microbial reductive processes. In *Biogeochemistry of Forested Catchments in a Changing Environment: A German Case Study*; Matzner, E., Ed.; *Ecological Studies*; Springer: Berlin, Heidelberg, 2004; pp 377−395.
(31) Paul, S.; Küsel, K.; Alewell, C. Reduction processes in forest wetlands: tracking down heterogeneity of source/sink functions with a combination of methods. *Soil Biol. Biochem.* **2006**, *38* (5), 1028−1039.
(32) Werner, B. J.; Musolff, A.; Lechtenfeld, O. J.; de Rooij, G. H.; Oosterwoud, M. R.; Fleckenstein, J. H. High-frequency measurements explain quantity and quality of dissolved organic carbon mobilization in a headwater catchment. *Biogeosciences* **2019**, *16* (22), 4497−4516.
(33) Pisani, O.; Bosch, D. D.; Coffin, A. W.; Endale, D. M.; Liebert, D.; Strickland, T. C. Riparian land cover and hydrology influence stream dissolved organic matter composition in an agricultural watershed. *Sci. Total Environ.* **2020**, *717*, 137165.
(34) Weishaar, J. L.; Aiken, G. R.; Bergamaschi, B. A.; Fram, M. S.; Fujii, R.; Mopper, K. Evaluation of specific ultraviolet absorbance as an indicator of the chemical composition and reactivity of dissolved organic carbon. *Environ. Sci. Technol.* **2003**, *37* (20), 4702−4708.
(35) Dittman, J. A.; Shanley, J. B.; Driscoll, C. T.; Aiken, G. R.; Chalmers, A. T.; Towse, J. E.; Selvendiran, P. Mercury dynamics in relation to dissolved organic carbon concentration and quality during high flow events in three Northeastern U.S. streams. *Water Resour. Res.* **2010**, *46* (7), W07522.
(36) Stoken, O. M.; Riscassi, A. L.; Scanlon, T. M. Association of dissolved mercury with dissolved organic carbon in U.S. rivers and streams: the role of watershed soil organic carbon. *Water Resour. Res.* **2016**, *52* (4), 3040−3051.
(37) Jiang, T.; Bravo, A. G.; Skyllberg, U.; Björn, E.; Wang, D.; Yan, H.; Green, N. W. Influence of dissolved organic matter (DOM) characteristics on dissolved mercury (Hg) species composition in sediment porewater of lakes from Southwest China. *Water Res.* **2018**, *146*, 146−158.
(38) Burns, D. A.; Aiken, G. R.; Bradley, P. M.; Journey, C. A.; Schelker, J. Specific ultra-violet absorbance as an indicator of mercury sources in an Adirondack River Basin. *Biogeochemistry* **2013**, *113* (1−3), 451−466.
(39) Dittman, J. A.; Shanley, J. B.; Driscoll, C. T.; Aiken, G. R.; Chalmers, A. T.; Towse, J. E. Ultraviolet absorbance as a proxy for total dissolved mercury in streams. *Environ. Pollut.* **2009**, *157* (6), 1953−1956.
(40) Graham, A. M.; Aiken, G. R.; Gilmour, C. C. Effect of dissolved organic matter source and character on microbial Hg methylation in Hg−S−DOM solutions. *Environ. Sci. Technol.* **2013**, *47* (11), 5746−5754.
(41) Peterson, B. D.; Krabbenhoft, D. P.; McMahon, K. D.; Ogorek, J. M.; Tate, M. T.; Orem, W. H.; Poulin, B. A. Environmental formation of methylmercury is controlled by synergy of inorganic mercury bioavailability and microbial mercury-methylation capacity. *Environ. Microbiol.* **2023**, *25* (8), 1409−1423.
(42) Haitzer, M.; Aiken, G. R.; Ryan, J. N. Binding of mercury(II) to dissolved organic matter: the role of the mercury-to-DOM concentration ratio. *Environ. Sci. Technol.* **2002**, *36* (16), 3564−3570.
(43) Amirbahman, A.; Reid, A. L.; Haines, T. A.; Kahl, J. S.; Arnold, C. Association of methylmercury with dissolved humic acids. *Environ. Sci. Technol.* **2002**, *36* (4), 690−695.
(44) Manceau, A.; Lemouchi, C.; Enescu, M.; Gaillot, A.-C.; Lanson, M.; Magnin, V.; Glatzel, P.; Poulin, B. A.; Ryan, J. N.; Aiken, G. R.; Gautier-Luneau, I.; Nagy, K. L. Formation of mercury sulfide from Hg(II)-thiolate complexes in natural organic matter. *Environ. Sci. Technol.* **2015**, *49* (16), 9787−9796.
(45) Graham, A. M.; Aiken, G. R.; Gilmour, C. C. Dissolved organic matter enhances microbial mercury methylation under sulfidic conditions. *Environ. Sci. Technol.* **2012**, *46* (5), 2715−2723.
(46) Seelen, E.; Liem-Nguyen, V.; Wünsch, U.; Baumann, Z.; Mason, R.; Skyllberg, U.; Björn, E. Dissolved organic matter thiol concentrations determine methylmercury bioavailability across the terrestrial-marine aquatic continuum. *Nat. Commun.* **2023**, *14* (1), 6728.
(47) Gerbig, C. A.; Kim, C. S.; Stegemeier, J. P.; Ryan, J. N.; Aiken, G. R. Formation of nanocolloidal metacinnabar in mercury-DOM-sulfide systems. *Environ. Sci. Technol.* **2011**, *45* (21), 9180−9187.
(48) Baldwin, A. K.; Janssen, S. E.; Tate, M. T.; Poulin, B. A.; Yoder, A. M.; Naymik, J.; Larsen, C.; Hoovestol, C.; Krabbenhoft, D. P. Mercury sources and budget for the Snake River above a hydroelectric reservoir complex. *Sci. Total Environ.* **2024**, *907*, 167961.
(49) Baldwin, A. K.; Poulin, B. A.; Naymik, J.; Hoovestol, C.; Clark, G. M.; Krabbenhoft, D. P. Seasonal dynamics and interannual variability in mercury concentrations and loads through a three-reservoir complex. *Environ. Sci. Technol.* **2020**, *54* (15), 9305−9314.
(50) Hoelscher, B.; Myers, R. *Tributary Pollutant Sources to the Hells Canyon Complex (No. Technical Report Appendix E.2.2-1). Hells Canyon Complex FERC No. 1971*; Idaho Power Company. 2003. https://docs.idahopower.com/pdfs/relicensing/hellscanyon/hellspdfs/techappendices/Water%20Quality/e22_01.pdf.
(51) Goodell, S. A. *Water Use on the Snake River Plain, Idaho and Eastern Oregon; U.S. Geological Survey Professional Paper 1408-E*; U.S. Geological Survey, 2023; p 63. https://pubs.usgs.gov/pp/1408e/report.pdf (accessed Nov 27, 2023).
(52) Dixon, M. D.; Johnson, W. C. Riparian vegetation along the Middle Snake River, Idaho: zonation, geographical trends, and historical changes. *Gt. Basin Nat.* **1999**, *59* (1), 18−34.
(53) Poulin, B. A.; Tate, M. T.; Ogorek, J.; Breitmeyer, S. E.; Baldwin, A. K.; Yoder, A. M.; Harris, R.; Naymik, J.; Gastelecutto, N.; Hoovestol, C.; Larsen, C.; Myers, R.; Aiken, G. R.; Krabbenhoft, D. P. Biogeochemical and hydrologic synergy control mercury fate in an arid land river-reservoir system. *Environ. Sci.: Processes Impacts* **2023**, *25* (5), 912−928.
(54) Hintelmann, H.; Wilken, R.-D. Levels of total mercury and methylmercury compounds in sediments of the polluted Elbe River: influence of seasonally and spatially varying environmental factors. *Sci. Total Environ.* **1995**, *166* (1−3), 1−10.
(55) Bento, B.; Hintelmann, H. Assessment of mercury methylation and methylmercury demethylation potentials in water and sediments along the Wabigoon River system. *Sci. Total Environ.* **2024**, *951*, 175658.
(56) Edwards, T. K.; Glysson, G. D. *Field Methods for Measurement of Fluvial Sediment; Open-File Report 86-531*; U.S. Geological Survey, 1988; p 132. https://pubs.usgs.gov/twri/twri3-c2/pdf/twri_3-C2_c.pdf (accessed Dec 07, 2023).
(57) Mueller, D. S. *QRev, U.S. Geological Survey Software Release*, 2020. https://doi.org/10.5066/P9OZ8QDL.
(58) Poulin, B. A.; Krause, V. M.; Baldwin, A. K.; Ogorek, J.; Tate, M. T.; Janssen, S. E.; Krabbenhoft, D. P.; Eagles-Smith, C. A.;

Willacker, J. J.; Pierce, J. R.; Yoder, A. M. *Hydrological, Chemical, and Biological Characterization of the Snake River and Associated Tributaries and Irrigation Drains from River Mile 448 to 346, 2022*, 2023, DOI: 10.5066/P9QWES6T.
(59) Kimball, B. A.; Runkel, R. L.; Walton-Day, K.; Bencala, K. E. Assessment of metal loads in watersheds affected by acid mine drainage by using tracer injection and synoptic sampling: Cement Creek, Colorado, USA. *Appl. Geochem.* **2002**, *17* (9), 1183−1207.
(60) Microsoft Corporation. *Microsoft Excel*, 2024. https://office.microsoft.com/excel.
(61) R Core Team. *R: A Language and Environment for Statistical Computing*, 2021. https://www.R-project.org/.
(62) Kassambara, A. *Rstatix: Pipe-Friendly Framework for Basic Statistical Tests*, 2023. https://rpkgs.datanovia.com/rstatix/.
(63) Helms, J. R.; Stubbins, A.; Ritchie, J. D.; Minor, E. C.; Kieber, D. J.; Mopper, K. Absorption spectral slopes and slope ratios as indicators of molecular weight, source, and photobleaching of chromophoric dissolved organic matter. *Limnol. Oceanogr.* **2008**, *53* (3), 955−969.
(64) Loux, N. T. An Assessment of mercury-species-dependent binding with natural organic carbon. *Chem. Speciation Bioavail.* **1998**, *10* (4), 127−136.
(65) Turner, A.; Millward, G. E.; Le Roux, S. M. Significance of oxides and particulate organic matter in controlling trace metal partitioning in a contaminated estuary. *Mar. Chem.* **2004**, *88* (3−4), 179−192.
(66) Marvin-DiPasquale, M.; Lutz, M. A.; Brigham, M. E.; Krabbenhoft, D. P.; Aiken, G. R.; Orem, W. H.; Hall, B. D. Mercury cycling in stream ecosystems. 2. benthic methylmercury production and bed sediment−pore water partitioning. *Environ. Sci. Technol.* **2009**, *43* (8), 2726−2732.
(67) Heyes, A.; Miller, C.; Mason, R. P. Mercury and methylmercury in Hudson River sediment: impact of tidal resuspension on partitioning and methylation. *Mar. Chem.* **2004**, *90* (1−4), 75−89.
(68) Du, H.; Ma, M.; Igarashi, Y.; Wang, D. Biotic and abiotic degradation of methylmercury in aquatic ecosystems: a review. *Bull. Environ. Contam. Toxicol.* **2019**, *102* (5), 605−611.
(69) Whalin, L.; Kim, E.-H.; Mason, R. Factors influencing the oxidation, reduction, methylation and demethylation of mercury species in coastal waters. *Mar. Chem.* **2007**, *107* (3), 278−294.
(70) Nealson, K. H.; Myers, C. R. Microbial reduction of manganese and iron: new approaches to carbon cycling. *Appl. Environ. Microbiol.* **1992**, *58* (2), 439−443.
(71) Gilmour, C. C.; Riedel, G. S.; Ederington, M. C.; Bell, J. T.; Gill, G. A.; Stordal, M. C. Methylmercury concentrations and production rates across a trophic gradient in the Northern Everglades. *Biogeochemistry* **1998**, *40* (2/3), 327−345.
(72) Tjerngren, I.; Karlsson, T.; Björn, E.; Skyllberg, U. Potential Hg methylation and MeHg demethylation rates related to the nutrient status of different boreal wetlands. *Biogeochemistry* **2012**, *108* (1−3), 335−350.
(73) Mitchell, C. P. J.; Branfireun, B. A.; Kolka, R. K. Spatial characteristics of net methylmercury production hot spots in peatlands. *Environ. Sci. Technol.* **2008**, *42* (4), 1010−1016.
(74) Tjerngren, I.; Meili, M.; Björn, E.; Skyllberg, U. Eight boreal wetlands as sources and sinks for methyl mercury in relation to soil acidity, C/N ratio, and small-scale flooding. *Environ. Sci. Technol.* **2012**, *46* (15), 8052−8060.
(75) Bradley, P. M.; Burns, D. A.; Murray, K. R.-.; Brigham, M. E.; Button, D. T.; Chasar, L. C.; Marvin-DiPasquale, M.; Lowery, M. A.; Journey, C. A. Spatial and seasonal variability of dissolved methylmercury in two stream basins in the Eastern United States. *Environ. Sci. Technol.* **2011**, *45* (6), 2048−2055.
(76) Poulin, B. A.; Gerbig, C. A.; Kim, C. S.; Stegemeier, J. P.; Ryan, J. N.; Aiken, G. R. Effects of sulfide concentration and dissolved organic matter characteristics on the structure of nanocolloidal metacinnabar. *Environ. Sci. Technol.* **2017**, *51* (22), 13133−13142.
(77) Jones, D. S.; Johnson, N. W.; Mitchell, C. P. J.; Walker, G. M.; Bailey, J. V.; Pastor, J.; Swain, E. B. Diverse communities of hgcAB+ microorganisms methylate mercury in freshwater sediments subjected to experimental sulfate loading. *Environ. Sci. Technol.* **2020**, *54* (22), 14265−14274.
(78) Neufeld, D. S. G. Mercury accumulation in caged corbicula: rate of uptake and seasonal variation. *Environ. Monit. Assess.* **2010**, *168* (1−4), 385−396.
(79) Subba, M.; Keough, M. J.; Kellar, C.; Long, S.; Miranda, A.; Pettigrove, V. J. *Potamopyrgus Antipodarum* has the potential to detect effects from various land use activities on a freshwater ecosystem. *Environ. Pollut.* **2021**, *287*, 117563.
(80) Kim, Y. G.; Kwon, S. Y.; Washburn, S. J.; Brooks, S. C.; Yoon, J. W.; Besnard, L. Reconsidering mercury sources and exposure pathways to bivalves: insights from mercury stable isotopes. *Water Res.* **2024**, *248*, 120843.
(81) Baldwin, A. K.; Eagles-Smith, C. A.; Willacker, J. J.; Poulin, B. A.; Krabbenhoft, D. P.; Naymik, J.; Tate, M. T.; Bates, D.; Gastelecutto, N.; Hoovestol, C.; Larsen, C.; Yoder, A. M.; Chandler, J.; Myers, R. In-reservoir physical processes modulate aqueous and biological methylmercury export from a seasonally anoxic reservoir. *Environ. Sci. Technol.* **2022**, *56* (19), 13751−13760.